Search for rare B meson decays at the *BABAR* experiment

R Cheaib

Department of Physics, University of Mississippi, 108 Lewis Hall, University MS 38677

E-mail: rachac@phys.olemiss.edu

Abstract. Flavour-changing neutral current (FCNC) processes, such as $b \to s$ transitions, play an important role in the search for physics beyond the Standard Model (SM). Contributions from virtual particles in the loop are predicted to deviate observables like the branching fraction, angular asymmetry, or CP-asymmetry from their SM expectations. Using data from the BaBar experiment, we present the first search for the rare decay $B^+ \to K^+ \tau^+\tau^-$. Furthermore, the *BABAR* results on the measurement of the angular asymmetries of $B \to K\ \ell^+\ell^-$, where ℓ = e or μ, are also reported. Specifically, the K^* longitudinal polarization and the forward-backward asymmetry is measured and presented. In addition, using a time-dependent analysis of $B \to K_S^0\pi^+\pi^-\gamma$, the mixing induced CP-asymmetry for the radiative FCNC decay $B \to K_S^0\rho\gamma$, is measured, along with an amplitude analysis of the $m_{K\pi}$ and $m_{K\pi\pi}$ spectrum.

1. Introduction

$b \to s$ transitions are highly suppressed in the SM and only occur via loop or box diagrams. Using an effective low-energy theory, the Lagrangian for $b \to s$ transitions, shown in equation 1, can be separated into two distinct parts: the long distance (low-energy) contrubutions contained in the operator matrix elements and the short-distance (high-energy) physics described the Wilson coefficients.

$$L = \frac{4G_F}{\sqrt{2}} V_{tb}V_{ts}^* \sum_{i=1}^{10} C_i(\mu)O_i(\mu) \tag{1}$$

where G_F is the fermi constant, V_{ij} are the relevant CKM matrix elements, C_i are the corresponding Wilson coefficients, and O_i are a complete set of renormalized operators involving the fields that govern $b \to s$ transitions [1]. Measurements of rare FCNC B meson decays are interesting since they can provide experimental constraints on the Wilson coefficients and are thus a stringent test of the SM. Furthermore, contributions to such decays from new-physics particles, like a charged Higgs or a supersymmetric particle [2], can modify the Wilson coefficients and require the introduction of new opertaor matrix elements. In fact, virtual particles in the loop allow one to probe, at relatively low energies, new physics at large mass scales.

The *BABAR* experiment [3][4] collected 424 fb^{-1} of data [5] by colliding electrons and positrons at the center-of-mass (CM) energy of the $\Upsilon(4S)$ resonance. The $\Upsilon(4S)$ decays into $B\overline{B}$ pair, resulting in more than 479 million $B\overline{B}$ events to study and analyze. Using the full *BABAR* dataset, a measurement of the $B^+ \to K^+\ \tau^+\tau^-$ branching fraction [6], $B \to K\ \ell^+\ell^-$ angular asymmetries [7] and $B \to K_S^0\rho\gamma$ mixing-induced CP-asymmetry [8] is performed.

2. Branching fraction measurement of $B^+ \to K^+ \tau^+\tau^-$

$B^+ \to K^+ \tau^+\tau^-$ [9] is a FCNC process with a braching fraction in the range 1-2 $\times 10^{-7}$ [10]. It is the third-lepton generation equivalent of $B \to K \ell^+\ell^-$, where $\ell = e$ or μ. The large mass of the τ lepton may provide improved sensitivity to new-physics contributions as compared to its light lepton counterparts [11][12]. For instance, in two-Higgs-doublet-models [13], the Higgs-lepton-lepton vertex is proportional to the mass of the τ and thus contributions to the total decay rate, as well as other observables, can be significant. The branching fraction of $B^+ \to K^+ \tau^+\tau^-$ is measured by exclusively reconstructing one B meson, referred to as the $B_{\rm tag}$, in the $\Upsilon(4S) \to B\overline{B}$ decay using hadronic modes, and then looking in the rest of the event for the $B^+ \to K^+ \tau^+\tau^-$ signal. This technique is referred to as the hadronic $B_{\rm tag}$ reconstruction, and is ideal for decays with missing energy . With exclusive reconstruction of the $B_{\rm tag}$, the four-vector of the other B, the $B_{\rm sig}$, can also be fully determined and thus the kinematics of the event are better constrained. Furthermore, the τ daughters of a given $B_{\rm sig}$ are required to decay only via leptonic modes: $\tau^- \to e^-\overline{\nu}_e\nu_\tau$ or $\tau^- \to \mu^-\overline{\nu}_\mu\nu_\tau$. Thus, there are three possible final states with e^+e^-, $\mu^+\mu^-$ or $e^+\ \mu^-$ in the final state, along with their associated neutrinos.

To select for $B^+ \to K^+ \tau^+\tau^-$ event, every event is required to have exactly one properly reconstructed charged $B_{\rm tag}$ with an energy substituted mass, $m_{\rm ES}$, that lies within the range of the mass of a B meson. The $m_{\rm ES}$ of a $B_{\rm tag}$ candidate is given by:

$$m_{\rm ES} = \sqrt{E^2_{\rm CM} - \vec{p}^{\,2}_{B_{\rm tag}}} \qquad (2)$$

where $E_{\rm CM}$ is half the total colliding energy and $\vec{p}_{B_{\rm tag}}$ is the 3-momentum of the reconstructed $B_{\rm tag}$, in the CM frame. To suppress backgrounds from continuum events where $e^+e^- \to q\overline{q}$ or $\ell^+\ell^-$, a multivariate likelihood selector based on six event shape variables is used. In a $B\overline{B}$ event, the produced B mesons are almost at rest and and thus their decay has an isotropic topology. On the other hand, the daughter quarks or leptons in a continuum event have high momenta, and the resulting decay topology is jet-like. The multivariate likelihood selector separates between the two classes of events and gets rid of more than 75% of the continuum background. Furthermore, $B^+ \to K^+ \tau^+\tau^-$ events are required to have nonzero missing energy, to account for the neutrinos in the leptonic decay of the τ lepton. The missing energy is calculated by subtracting all signal side tracks and clusters from the $B_{\rm sig}$. A signal event is required to have 3 tracks, one satisfying the particle identification criteria of a K and the remaining two of an electron or muon. In addition, the presence of the massive τ leptons imposes an upper limit on the K momentum. This pushes the s_B distribution, where $s_B = (p_{B_{\rm sig}} - p_K)^2/m_B^2$, of signal events to higher values, as compared with background events, and thus a requirement of $s_B > 0.45$ is applied. At this point, the main source of background is from combinatorial events with semi-leptonic charmed B decays, such as $B \to D^{(*)}\ell\nu_e, D^{(*)} \to K\ell\nu_e$. To suppress this background, a multi-layer perceptron neural network, consisting of eight discriminating variables such as the angle between the lepton and the oppositely charged kaon in the $\tau^+\tau^-$ rest frame , is used. The neural network is then trained and tested for each of the three signal channels, and the combined MLP output is shown in Fig. 1. The final step in the signal selection is a requirement on the MLP output for each signal channel.

The final background estimate after the MLP cut is divided into two parts: combinatorial and $m_{\rm ES}$-peaking. The former represents the continuum and $B^0\overline{B}^0$ background events, which do not have a peaking $m_{\rm ES}$ distribution, and is estimated using data in the $m_{\rm ES}$ sideband region, defined as $5.20 < m_{\rm ES} < 5.26\,{\rm GeV}/c^2$. The latter is determined using B^+B^- simulated Monte Carlo samples, which consist mainly of semi-leptonic B decays and is scaled by a $B_{\rm tag}$ yield correction to account for any discrepancies between data and MC. The level of data-MC agreement is cross-checked by running a $B^+ \to D^0\ell\nu_e, D^0 \to K^-\pi^+$ control sample through the MLP neural network and verifying the output distributions. The control sample is also used to determine the systematic uncertainty associated with the neural network used in the signal

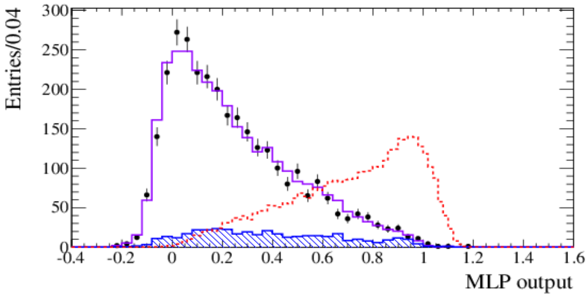

Figure 1. (color online) MLP output distribution for the $B^+ \to K^+\tau^+\tau^-$ analysis. The signal MC distribution is shown (dashed) with arbitrary normalization, along with the data (points) and the expected combinatorial (shaded) plus $m_{\rm ES}$-peaking (solid) background contributions.

selection. Other sources of systematic uncertainties include particle identification and the $B_{\rm tag}$ yield correction. The final data yield is determined seperately for each of the three $B^+ \to K^+ \tau^+\tau^-$ signal channels. The yields in the e^+e^- and $\mu^+\mu^-$ channels show consistency with the background estimate, while a 3.7 σ excess is obesrved in the e^+ μ^- channel. Examination of the input and output distributions of the e^+ μ^- channels does not show any clear evidence of signal-like behaviour or any mis-modelling of the background. Given that the combined excess is less than 2 σ and that the kinematic distributions of the e^+ μ^- channel does not show any clear evidence of signal-like behaviour, the observed excess is not interpreted as signal. The combined upper limit at the 90% confidence level is $< 2.6 \times 10^{-3}$. This is the first measurement of $B^+ \to K^+ \tau^+\tau^-$.

3. Angular asymmetries in $B \to K\ \ell^+\ell^-$

$B \to K^*\ \ell^+\ell^-$ is also a FCNC process, with an amplitude expressed in terms of hadronic form factors and the C_7, C_9, and C_{10} Wilson Coefficients[7]. The angular distributions of $B \to K^*$ $\ell^+\ell^-$, specifically the K^* longitudinal polarization, F_L, and the forward-backward asymmetry, A_{FB}, are notably sensitive to physics beyond the SM [14]-[15] and have been previously measured by various experiments [16]-[20].

At any given value of the q^2, the kinematic distribution of the $B \to K^*\ell^+\ell^-$ decay products can be expressed in terms of three distinct angles: θ_K, the angle between the K and the B in the K^* rest frame, θ_l, the angle between the lepton and the B in the $\ell^+\ell^-$ rest frame, and ϕ, the angle between the $\ell^+\ell^-$ and $K\pi$ decay planes in the B rest frame [7]. After integrating out ϕ and θ_l, F_L can be determined using a fit to $\cos\theta_K$ of the form [21]:

$$\frac{3}{2}F_L(q^2)\cos^2\theta_K + \frac{3}{4}(1 - F_L(q^2))(1 - cos^2\theta_K) \tag{3}$$

Similarly, A_{FB} can be extracted using a fit to θ_l after integrating over ϕ and θ_K [21]:

$$\frac{3}{4}F_L(q^2)(1 - cos^2\theta_l) + \frac{3}{8}(1 - F_L(q^2))(1 + cos^2\theta_l) + A_{FB}(q^2)\cos\theta_l. \tag{4}$$

To measure F_L and A_{FB}, $B \to K^*\ \ell^+\ell^-$ signal events are reconstructed in one of the following final states : K^{*+} $(\to K^0_S\ \pi^+)\mu^+\mu^-$, K^{*0} $(\to K^+\ \pi^-)\mu^+\mu^-$, K^{*+} $(\to K^+\ \pi^0)e^+e^-$, K^{*+} $(\to K^0_S\ \pi^+)e^+e^-$, K^{*0} $(\to K^+\ \pi^-)e^+e^-$. Each K^* candidate is required to have an invariant mass $0.72 < m_{K\pi} < 1.10\,{\rm GeV}/c^2$, while the leptons are required to have momenta greater than 0.3 GeV/c^2. The $m_{\rm ES}$ and ΔE of the resulting B candidate is then determined and used to separate

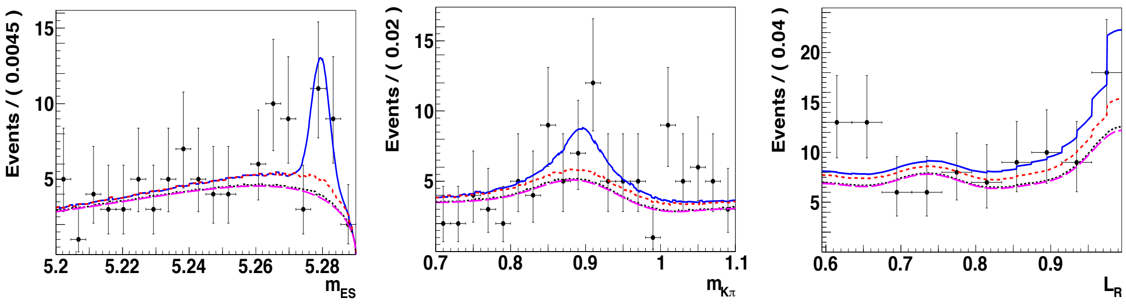

(a) $m_{\rm ES}$: $B^0 \to K^+\pi^-e^+e^-$.   (b) $m_{K\pi}$: $B^0 \to K^+\pi^-e^+e^-$.   (c) L_R: $B^0 \to K^+\pi^-e^+e^-$.

Figure 2. 3-D fit projections for $B^0 \to K^+\ \pi^-\ e^+e^-$ in q_5^2. Each event class is shown: combinatorial (magenta long dash) and charmonium (black dots) background events, crossfeed signal events (red short dash) and total (solid blue) pdf.

between signal and background. Here, $\Delta E = E_B^* - E_{CM}/2$, where E_B^* is the energy of the B in the CM frame and E_{CM} is total CM energy. The main source of background is from semileptonic B and D decays, as well as continuum background with random combinations of leptons. Eight bagged decision trees (BDT) are trained to suppress these $B\overline{B}$ and $q\overline{q}$ backgrounds. Various BDT input variables are used, including the magnitude of the total transverse momentum, the mass of the other B meson in the event, the ratio of the Fox-Wolfram moments R_2 [22]. A final requirement on ΔE and L_R is applied at the end of the signal selection: $-0.1(0.05) < \Delta E < 0.05$ for the e^+e^- $(\mu^+\mu^-)$ modes, $L_R > 0.6$. Here, L_R is a likelihood ratio which uses the output of the $B\overline{B}$ BDT to determine how likely a given event is signal vs background.

To extract the angular observables, the q^2 spectrum is divided into five disjoint bins $(q_1 - q_5)$ of varying size, and an additional bin q_0, ranging between 1.0 and 6.0 GeV $^2/c^4$. An initial unbinned maximum likelihood fit of $m_{\rm ES}$, $m(K\pi)$, and L_R is performed to fix the normalizations and shapes of all probability density functions (pdfs) dependent on these three variables. Second, for each mode and each q^2 bin, the 3-D likeihood fit is used to fix the normalizations of events with $m_{\rm ES} > 5.27\,{\rm GeV}/c^2$. Third, $\cos\theta_K$ is added as a fourth dimension to the likelihood function, and four-dimensional likelihoods are defined for each signal mode and each q^2 with F_L as the only free parameter. Finally, the fitted value of F_L is then used as input to a similar 4-D fit, where $\cos\theta_l$ has been added as a fourth dimension instead of $\cos\theta_K$. The pdfs in the likelihood fit are defined for five different event classes: true signal events, crossfeed signal events, combinatorial backgrounds, backgrounds from charmonium decays, and finally backgrounds from hadronic decays which are only prominent for $\mu^+\mu^-$ modes. Fig. 2 shows the initial 3-D fit projections for $B^0 \to K^+\ \pi^-\ e^+e^-$ in q_5^2 with the different event classes. F_L and A_{FB} are extracted in each q^2 bin for the charged, $B^+ \to K^{*+}\ \ell^+\ell^-$, neutral, $B^0 \to K^{*0}\ \ell^+\ell^-$, and total $B \to K^*\ \ell^+\ell^-$ modes. The results are shown in Fig. 3, along with previous Belle [16], CDF [17], LHCb [18], and CMS [19].

As can be readily seen, the $B^0 \to K^{*0}\ \ell^+\ell^-$ results show good agreement with the SM expectations and other experiments. For the charged mode, the value of F_L is relatively small in the low q^2 region and thus exhibits tension with the SM expecation. An additional angular observable P_2 is defined such that $P_2 = (-2/3) \times A_{FB}/(1 - F_L)$. P_2 has diminished theoretical uncertainty and thus higher sensitvity to non-SM contributions. The tension at low q^2 is still found in the P_2 distribution and can be a hint of new physics, specifically result is consistent with the existence of right-handed currents. This is the first measurement of angular asymmetries in $B^+ \to K^{*+}\ \ell^+\ell^-$.

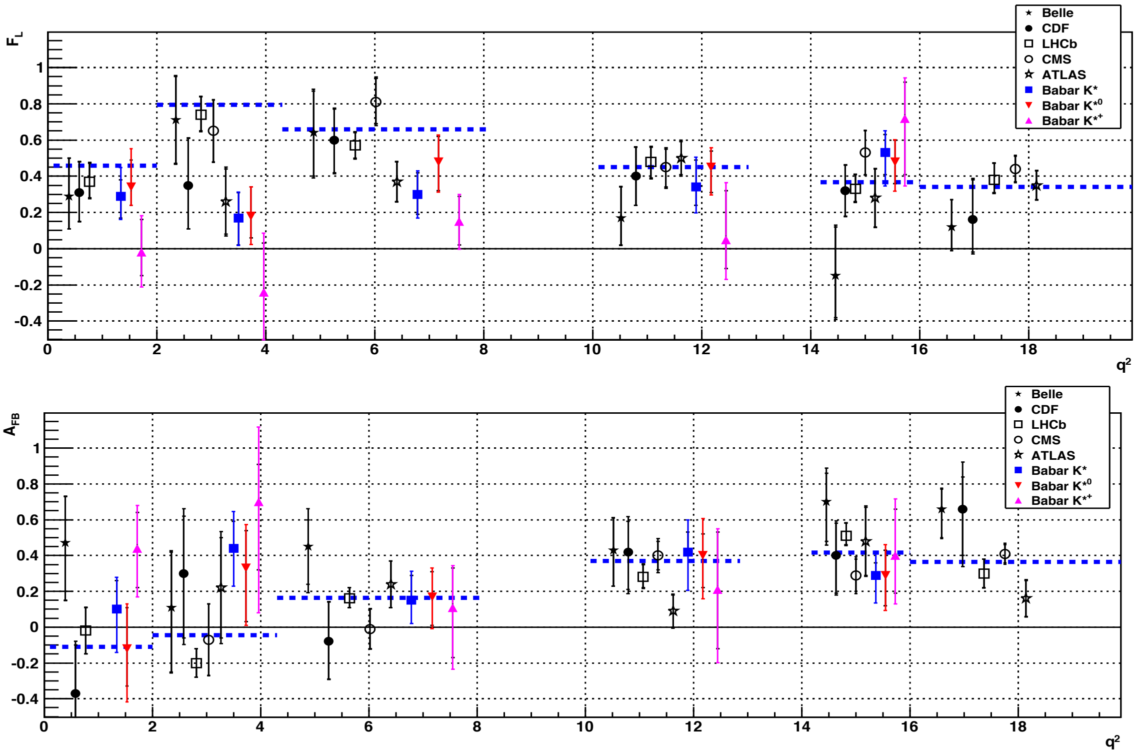

Figure 3. F_L and A_{FB} results for charged (magenta filled pointing-up triangle), neutral (red filled down-pointing triangle) and total $B \to K^* \ \ell^+\ell^-$ (blue filled square) in disjoint q^2 bins. The SM expectations are shown as blue dashed lines along with results from other experiments: Belle [16] (black filled star), CDF [17] (black filled circle), LHCB [18] (black open square), CMS [19] (black open circle), and ATLAS [20] (black open star).

4. Mixing induced CP-asymmetry, S_{fCP}, in $B \to K^0_S\rho\gamma$

In the SM, the photon emitted in $b \to s\gamma$ transitions is predominantly left-handed, with contamination from right-handed photons suppressed by a factor of m_s/m_b [23]. This implies that B^0 ($\overline{B}^0$) mesons decay predominantly to right-handed (left-handed) photons and the mixing-induced CP-asymmetry in $B \to f_{CP}\gamma$ decays is expected to be small. However, various new physics models [24]-[25] introduce enhanced contributions from right-handed photons and thus alter the prediction of a small CP-asymmetry.

In this analysis, the mixing-induced CP-asymmetry of $B^0 \to K^0_S\rho\gamma$, $S_{K^0_S\rho\gamma}$, is measured using a time-dependent analysis of $B^0 \to K^0_S\pi^+\pi^-\gamma$. Due to the large natural width of the ρ meson, there is an irreducible contribution from the non-CP eigenstate $B^0 \to K^{*\pm}(\to K^0_S\pi^\pm)\pi^\mp\gamma$ which affects $S_{K^0_S\rho\gamma}$, and thus a dilution factor, $D_{K^0_S\rho\gamma} \equiv S_{K^0_S\pi^+\pi^-\gamma}/S_{K^0_S\rho\gamma}$, must be determined. Here, $S_{K^0_S\pi^+\pi^-\gamma}$ is the effective value of the mixing-induced CP asymmetry for the full $B^0 \to K^0_S\pi^+\pi^-\gamma$ dataset. To determine $D_{K^0_S\rho\gamma}$, an amplitude analysis of the $m_{K\pi}$ spectra must be performed. Given the small number of events expected in the $B^0 \to K^0_S\pi^+\pi^-\gamma$ sample, the amplitudes of the resonant modes are extracted from the charged $B^+ \to K^+\pi^+\pi^-\gamma$ mode instead, under the assumption of isospin asymmetry, and extracted to the neutral mode. Furthermore, because the decay to the $K^+\pi^+\pi^-\gamma$ final state proceeds in general through three-body resonances first which then further decay into their $K^*\pi$ or $K\rho$ components, it is necessary to determine the three-body resonance content of the $m_{K\pi\pi}$ spectrum as well.

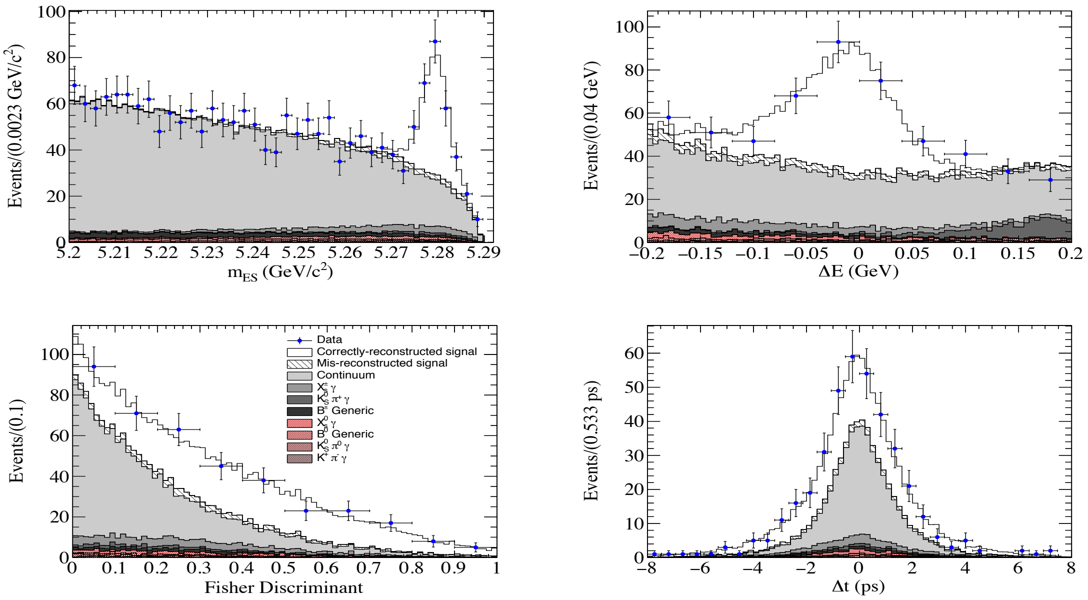

Figure 4. Distributions of m_{ES} (top left), ΔE, Fisher discriminant output F, and Δt with the fit results for the $B^0 \to K^0_S\pi^+\pi^-\gamma$ data sample. The data is shown as points with error bars and the stacked histograms represent the different background contributions.

$B^+ \to K^+\pi^+\pi^-\gamma$ events are reconstructed from one high energy photon with $1.5 < E_\gamma < 3.5\,\mathrm{GeV}$, two oppositely-chared pions, and one charged kaon. These are combined to form a B candidate, whose m_{ES} should lie with 5.20 and 5.92 GeV/c^2 and $|\Delta E| < 0.200\,\mathrm{GeV}$. A Fisher discriminant, consisting of six discriminating variables, is trained to suppress continuum background events. Furthermore, to reduce backgrounds from photons that originate from π^0 or η decay, a likelihood ratio, L_R, is constructed. With L_R, each photon candidate is associated with all other photons in the event and the probability of it originating from a π^0/η decay is determined. To extract the $B^+ \to K^+\pi^+\pi^-\gamma$ yield, an unbinned extended maximum likelihood fit to the m_{ES}, ΔE, and Fisher discriminat output F is performed. The resulting yield is $2441 \pm 9^{+41}_{-54}$ events, which translates into a branching fraction of $\mathcal{B}(B^+ \to K^+\pi^+\pi^-\gamma) = (24.5 \pm 0.9 \pm 1.2) \times 10^{-6}$.

The $m_{K\pi\pi}$ spectrum is then extracted from the maximum likelihood fit, and modeled as the coherent sum of five kaonic Breit-Wigner resonances: $K_1(1270), K_1(1400), K^*(1410), K^*(1680)$ and $K^*_2(1430)$. The fit fraction of each resonance is determined and the corresponding branching fraction, given by $\mathcal{B}(B^+ \to K_{res}(\to K^+\pi^+\pi^-)\gamma)$, is computed. Furthermore, a binned maximum likelihood fit is then performed to the efficiency-corrected $m_{K\pi}$ spectrum. Using the phasespace decay of the three-body resonances $m_{K\pi\pi}$, an efficiency map is determined and applied to the $m_{K\pi}$ spectrum. The latter is modeled as the projection of two 1^- P-wave components, $K^*(892)$ and $\rho(770)$, and one 0^+ S-wave component, $(K\pi)^{(*0)}_0$. The branching fractions $\mathcal{B}(B^+ \to K_{res}\pi^+\gamma)$ are also determined. Many of the measured branching fractions in this analysis are the first to be done or more accurate that previous world averages. Using the results of the $m_{K\pi}$ spectrum, the dilution factor is computed and yields $D_{K^0_S\rho\gamma} = -0.78^{+0.19}_{-0.17}$.

To measure the time-dependent CP asymmetry, the proper-time difference, given by $\Delta t = t_{rec} - t_{tag}$, is determined, between a fully reconstructed $B^0 \to K^0_S\rho\gamma$ decay (B^0_{rec}) and the other B in the event B_{tag}, which is partially reconstructed. The distance between the decay-vertex positions of B_{tag} and B_{rec} is measured and transformed to ΔE using the boost $\beta\gamma = 0.56$ of the

e^+e^- system. A B-flavor tagging algorithm [26] is used, which combines various event variables to achieve optimal separation between the two B candidates in a signal event. $B^0 \to K_S^0\pi^+\pi^-\gamma$ events are reconstructed using the same signal selection as $B^+ \to K^+\pi^+\pi^-\gamma$, but with $K_S^0 \to \pi^+\pi^-$. An unbinned maximum likelihood fit is then performed to the $m_{\rm ES}$, ΔE, Fisher discriminant output, Δt and $\sigma_{\Delta t}$ distributions to extract the signal yield. The fit is shown in Fig 4 and yields $N_{sig} = 243 \pm 24^{+21}_{-17}$ and thus a branching fraction $\mathcal{B}(B^0 \to K^0\pi^+\pi^-\gamma) = (20.5 \pm 2.0^{+2.6}_{-2.2}) \times 10^{-6}$. The CP-violation parameters are then determined to be $S_{K_S^0\pi^+\pi^-\gamma} = 0.14 \pm 0.25 \pm 0.03$ and $C_{K_S^0\pi^+\pi^-\gamma} = -0.29 \pm 0.20^{+0.03}_{-0.02}$. Using the calculated dilution factor and assuming isospin asymmetry, the resulting time-dependent CP asymmetry for $B^0 \to K_S^0\rho\gamma$ is calculated to be: $S_{K_S^0\rho\gamma} = -0.18 \pm 0.32^{+0.06}_{-0.05}$. This measurement is in agreement with previously published results [27]-[29] and shows no deviation from the SM prediction.

5. Conclusion

Various interesting and leading results are still being produced using the *BABAR* dataset. The branching fraction of $B^+ \to K^+ \tau^+\tau^-$ has been measured for the first time. Furthermore, the angular asymmtries in $B \to K^* \ell^+\ell^-$ are measured and display tension with the SM expectations in the low q^2 region. In addition, the time-dependent CP-asymmetry in $B \to K_S^0\rho\gamma$ has been measured and shows consistency with the SM. $b \to s$ transitions continue to be a promising probe of physics beyond the SM and a point of interest for current and future B-factories.

[1] A. J. Bevan *et al.* [*BABAR* and Belle Collaborations], Eur. Phys. J. C**74**, 3026 (2014).
[2] T. M. Aliev , M. Savci and A. Ozpineci, J. Phys. G **24**, 49 (1998).
[3] B. Aubert *et al.* [*BABAR* Collaboration], Nucl. Instrum. Meth. A **479**, 1 (2002);
[4] B. Aubert *et al.* [*BABAR* Collaboration], Nucl. Instrum. Meth. A **729**, 615 (2013).
[5] J. P. Lees *et al.* [*BABAR* Collaboration], Nucl. Instrum. Meth. A **726**, 203 (2013).
[6] arXiv:1605.09637
[7] J. P. Lees *et al.*[*BABAR* Collaboration], Phys. Rev. D **93**, 052015 (2016).
[8] J. P. Lees *et al.* [*BABAR* Collaboration], Phys. Rev. D **93**, 052013 (2016).
[9] The charge conjugate mode $B^- \to K^- \tau^+\tau^-$ is also implied.
[10] C. Bouchard, G. P. Lepage, C. Monahan, H. Na and J. Shigemitsu, Phys. Rev. Lett. **111**, 162002 (2013).
[11] Q. Yan *et al.*, Phys. Rev. D **62**, 094023 (2000).
[12] D. Guetta and E. Nardi, Phys. Rev. D **58**, 012001 (1998).
[13] T. M. Aliev , M. Savci and A. Ozpineci, J. Phys. G **24**, 49 (1998).
[14] T. Feldmann and J. Matias, JHEP **0301**, 074 (2003).
[15] Y. G. Xu, R. M. Wang and Y.D. Yang, Phys. Rev. D **74**, 114019 (2006).
[16] J. T. Wei *et al.* [Belle Collaboration], Phys. Rev. Lett. **103**, 171801 (2009).
[17] T. Aaltonen *et al.* [CDF Collaboration], Phys. Rev. Lett. **108**, 081807 (2012).
[18] R. Aaij *et al.* [LHCb Collaboration], JHEP **1308**, 131 (2013).
[19] S. Chatrchyan *et al.* [CMS collaboration], Phys. Lett. B **727**, 77 (2013).
[20] G. Aad *et al.* [ATLAS Collaboration], ATLAS-CONF-2013-038.
[21] F. Kruger and J. Matias, Phys. Rev. D **71**, 094009 (2005).
[22] G. C. Fox and S. Wolfram, Phys. Rev. Lett. **89**, 281802 (2002).
[23] D. Atwood, M. Gronau and A. Soni, Phys. Rev. Lett. **79**, 185 (1997).
[24] K. Fujikawa and A. Yamada, Phys. Rev. D **49**, 5890 (1994).
[25] P. L. Cho and M. Misiak, Phys. Rev. D **49**, 5894 (1994).
[26] B. Aubert *et al.* [*BABAR* Collaboration], Phys. Rev. Lett. **99**, 171803 (2007).
[27] J. Li *et al.* [Belle Collaboration], Phys. Rev. Lett. **101**, 251601 (2008).
[28] B.Aubert *et al.* [*BABAR* Collaboration], Phys. Rev. D **78**, 071101 (2008).
[29] Y. Ushiroda *et al.* [Belle Collaboration], Phys. Rev. D **74**, 111104 (2006).